

## A MONTE CARLO APPROACH TO MAGNETAR-POWERED TRANSIENTS: II. BROAD-LINED TYPE IC SUPERNOVAE NOT ASSOCIATED WITH GRBS

L. J. WANG<sup>1</sup>, Z. CANO<sup>2,3</sup>, S. Q. WANG<sup>4,5,6</sup>, W. K. ZHENG<sup>6</sup>, H. YU<sup>4,5</sup>, L. D. LIU<sup>4,5</sup>, Y. H. HAN<sup>1</sup>, Z. G. DAI<sup>4,5</sup>, D. XU<sup>1</sup>, Y. L. QIU<sup>1</sup>, J. Y. WEI<sup>1</sup><sup>1</sup>Key Laboratory of Space Astronomy and Technology, National Astronomical Observatories, Chinese Academy of Sciences, Beijing 100012, China; wanglj@nao.cas.cn, wjy@nao.cas.cn<sup>2</sup>Instituto de Astrofísica de Andalucía (IAA-CSIC), Glorieta de la Astronomía s/n, E-18008, Granada, Spain.<sup>3</sup>Juan de la Cierva Fellow.<sup>4</sup>School of Astronomy and Space Science, Nanjing University, Nanjing 210093, China; dzg@nju.edu.cn<sup>5</sup>Key Laboratory of Modern Astronomy and Astrophysics (Nanjing University), Ministry of Education, Nanjing 210093, China and<sup>6</sup>Department of Astronomy, University of California, Berkeley, CA 94720-3411, USA

Draft version February 13, 2017

## ABSTRACT

The explosion mechanism of broad-lined type Ic supernovae (SNe Ic-BL) is not very well understood despite their discovery more than two decades ago. Recently a serious confrontation of SNe Ic-BL with the magnetar (plus <sup>56</sup>Ni) model was carried out following previous suggestions. Strong evidence for magnetar formation was found for the well-observed SNe Ic-BL 1998bw and 2002ap. In this paper we systematically study a large sample of SNe Ic-BL not associated with gamma-ray bursts. We use photospheric velocity data determined in a self-consistent way, which is an improvement to previous methods that suffered from large inconsistencies. We find that the magnetar+<sup>56</sup>Ni model provides a good description of the light curves and velocity evolution of our sample of SNe Ic-BL, although some SNe (not all) can also be described by the pure-magnetar model or by the pure-<sup>56</sup>Ni (two-component) model. In the magnetar model, the amount of <sup>56</sup>Ni required to explain their luminosity is significantly reduced, and the derived initial explosion energy is, in general, in accordance with neutrino heating. Some correlations between different physical parameters are evaluated and their implications regarding magnetic field amplification and the total energy reservoir are discussed.

*Subject headings:* stars: neutron — supernovae: general — supernovae: individual (SNe 1997ef, 2002ap, 2003jd, 2007bg, 2007ru, 2009bb, 2010ah, 2010ay, 2012ap, PTF10qts, PTF10vgv)

## 1. INTRODUCTION

Over the past two decades, the discovery of broad-lined type Ic supernovae (SNe Ic-BL; see Filippenko 1997, for the classification of known SNe) and superluminous SNe (SLSNe) has greatly enlarged the family of known core-collapse SNe (CCSNe). The association between long-duration gamma-ray burst (GRB) 980425 and its spectroscopically associated Ic-BL SN 1998bw (Galama et al. 1998; Patat et al. 2001), i.e. the so-called GRB-SN connection (Woosley & Bloom 2006; Cano et al. 2016b), ignited interest in these energetic and rare type of stripped-envelope CCSNe.

To date, the luminosity of most, if not all, GRB-SNe and SNe Ic-BL could be explained by radioactive heating arising from energy deposition from the radioactive decay of nickel and cobalt, which is nucleosynthesized during the explosion, into their daughter products (Cano et al. 2016a). However, it appears that the luminosity of many SLSNe cannot be adequately explained in this scenario, and alternative energy sources have been proposed. As a consequence, it is now usually assumed that at least a subclass of SLSNe, type Ic SLSNe, are powered by millisecond magnetars (Kasen & Bildsten 2010; Woosley 2010; Chatzopoulos et al. 2012; Inerra et al. 2013; Nicholl et al. 2014; Metzger et al. 2015; Mösta et al. 2015; Wang et al. 2015a; Dai et al. 2016; Kashiyama et al. 2016) although there is evidence for interaction between ejecta and circumstellar medium (Yan et al. 2015;

Wang et al. 2016e) at late times.

For SNe Ic-BL, shortcomings of one-dimensional <sup>56</sup>Ni model (e.g., Iwamoto et al. 2000; Nakamura et al. 2001) stimulated the suggestion for a two-component <sup>56</sup>Ni model (Maeda et al. 2003). In this model it is assumed that the ejecta are composed of two components, the outer fast-moving component (jet) and the inner slow-moving component (core). The former is responsible for the bright peak of the light curve, while the latter is responsible for the late-time exponential decay. This model is very useful for providing a better description of the ejecta structure and has been very successful in reproducing the luminosity of all SNe Ic-BL.

It is only recently that the application of the magnetar model to SNe Ic-BL was seriously considered (Cano et al. 2016a; Wang et al. 2016b,c,d), following the early suggestions (Ostriker & Gunn 1971; Wheeler et al. 2000; Thompson et al. 2004; Woosley 2010). The proposition of the improved magnetar model (Wang et al. 2016c), which takes into account the photospheric recession and acceleration of the ejecta by the spinning-down magnetar, provides an opportunity to examine the magnetar model against SNe Ic-BL in a self-consistent way. It was shown that the spin-down of the magnetar will lose a small fraction of its rotational energy to its light curve (Wang et al. 2016b), while the remaining fraction is transferred into the kinetic energy of the ejecta. Evidence for the formation of stable magnetars following the explosions of SNe

Ic-BL was subsequently found by Wang et al. (2016d). Such a model can also naturally account for the mysterious origin of the huge kinetic energies of SNe Ic-BL (Wang et al. 2016b).

The discovery of relativistic SNe Ic-BL, 2009bb and 2012ap, through their bright late-time radio emission (Bietenholz et al. 2010; Soderberg et al. 2010; Chakraborti et al. 2011, 2015) places the magnetar model on a more solid ground because such events require central engines to accelerate a tiny fraction of the ejecta to quasi-relativistic velocities (Margutti et al. 2014). Actually there is a continuous distribution of various types of CCSNe on the kinetic energy profile of the ejecta. The relativistic SNe Ic-BL lie in between ordinary SNe Ibc and energetic GRBs and are similar to the sub-energetic GRBs, e.g. GRB 100316D (Margutti et al. 2013) and GRB 140606B (Cano et al. 2015). This may indicate that similar engines were operating in sub-energetic GRBs and SNe 2009bb and 2012ap.

Based on the above findings, here we test the hypothesis that all of SNe Ic-BL are powered by magnetars. Under such hypothesis, we assessed the validity of the derived fitting parameters and consider the statistical characteristics of SNe Ic-BL. Despite the paucity of observed SNe Ic-BL, the accumulation of such events has reached a level where a meaningful statistical results can start to be obtained. It is therefore very timely to confront a larger sample ( $N = 11$ ) of SNe Ic-BL with the magnetar model.

To determine the uncertainties in the fitting parameters, Wang et al. (2016d) developed a Markov chain Monte Carlo (MCMC) code on the basis of the magnetar model. This code was applied to SLSNe Ic (Liu et al. 2017) to minimize the total errors arising from fitting the model to the SN light curves, and evolution of photospheric velocity and temperature, if available. In this paper we focus on the SNe Ic-BL not associated with GRBs. In what follows we use the words “SNe Ic-BL” to indicate SNe Ic-BL not associated with GRBs except when specifically mentioned otherwise.

The structure of this paper is as follows. In Section 2 we present the data available in the literature, along with a detailed analysis on the uncertainties of the data. Then in Section 3 we present our fitting results of the known SNe Ic-BL. Section 4 discusses the implications of the results. Particularly, Section 4.2 discusses the estimation of the appearance of nebular features by early light curve modeling; Section 4.3 discusses the correlations between the derived parameters; Section 4.4 discusses the possibility of alternative models to interpret the light curves and velocity evolution of some SNe. A summary is given in Section 5.

## 2. DATA ANALYSIS

Modjaz et al. (2016) listed 12 SNe Ic-BL. However, the light curve of SN 2007D is missing and we are therefore left with 11 such events, as listed in Table 1. We read the relevant literature carefully, and found that the bolometric light curves are acquired by different assumptions because of the frequent lack of some observational bands. To construct a bolometric light curve, emission in passbands *UV* (ultraviolet), *BVRI* (optical) and *IR* (UVOIR) should be integrated. It is, however, commonplace that only the optical bands are available for the

follow-up of a SN from very early times to late times. *UV* emission of a SN Ic-BL is usually strongest only at early stages, and its contribution to the total UVOIR bolometric flux can be more than 20% during the first two weeks (Cano et al. 2011; Lyman et al. 2014), while late-time *UV* follow-up is frequently missing. *IR* emission, which is usually strong for the whole evolution stage (and can contribute as much as 50% of the total UVOIR bolometric flux after peak light, e.g., Figure 6 of Tomita et al. 2006 and Figure 7 of Olivares & Finkbeiner et al. 2015), is only obtained for a few SNe. For this reason, we list the different assumptions and observational bands in Table 1.

Another uncertainty in the construction of a bolometric light curve comes from the treatment of extinction. The Galactic extinction is well-understood and can be handled properly using the dust maps of Schlegel et al. (1998), and as revised by Schlafly & Finkbeiner (2011). The host extinction, however, can only be estimated for some SNe because of the poor quality of the Na I D lines in the measured spectra (which may be a poor proxy for the host extinction anyways, e.g., Poznanski et al. 2011). We list the extinction treatment in Table 1. Even for the same SN, the determined extinction could be different from different authors. Taking SN 2012ap as an example, Milisavljevic et al. (2015) adopted a total extinction of  $E(B - V)_{\text{total}} = 0.45$  mag, while Liu et al. (2015) adopted a value of  $E(B - V)_{\text{total}} = 0.87$  mag.

Further uncertainty comes from the different values of the cosmological parameters used in the literature to derive the luminosity distances to the various SNe. For SNe 2002ap, 2009bb, 2012ap, redshift-independent methods, e.g. Tully-Fisher measurements, were facilitated to derive the distances, as are available on NASA/IPAC Extragalactic Database (NED). Such linear distances are weightedly averaged, as listed in Table 1. For other SNe that no such linear distances are available, to minimize distance uncertainties, we transform, according to the method described in Cano et al. (2014), the light curves in the literature to a common cosmology, i.e. the latest Planck results:  $H_0 = (67.8 \pm 0.9) \text{ km s}^{-1} \text{ Mpc}^{-1}$ ,  $\Omega_m = 0.308 \pm 0.012$  (Ade et al. 2016).

To compare the differences in distances, we also list the distances used in the original papers. Nevertheless, because the redshifts of the SNe studied here are small (see Table 2 in Modjaz et al. 2016), it is found that the errors in the infrared-derived distances introduced by assuming different cosmological parameters are small, typically 3 – 5%. Corsi et al. (2012) did not give the distance modulus of PTF10vgv in their derivation of absolute magnitudes. We digitalized their Figure 2 and found  $\mu_{\text{PTF10vgv}} = 33.9$  mag, based on which the light curve transformation was performed. In summary, the largest difference between our adopted distance and that used in the original paper is for SN 2002ap, for which we adopt 9.22 Mpc, rather than 7.94 Mpc in the original paper. The smallest difference is for SNe 2009bb, for which distances  $\sim 40$  Mpc have been adopted in the relevant studies.

The photospheric velocity is another critical quantity that significantly impacts the light curve fitting results. Different velocity indicators in the spectra, e.g. Si II  $\lambda 6355$ , Na I D  $\lambda 5891$ , O I  $\lambda 7774$ , Ca II  $\lambda 8579$ , Fe II  $\lambda 5169$ , usually give different results (Valenti et al. 2008; Mod-

TABLE 1  
THE SNe Ic-BL SAMPLE

SN	References		Extinction <sup>a</sup> corrected	Bands <sup>b</sup> integrated	Luminosity distance		
	Light curve	Velocity			original <sup>c</sup> (Mpc)	method <sup>d</sup>	adopted <sup>e</sup> (Mpc)
1997ef	I00	M16	None	NS	52.3	C	50.6
2002ap	T06	M16	GH	OIR	7.94	L	9.22
2003jd	V08	M16	GH	UVOIR <sup>f</sup>	78	C	84.3
2007bg	Y10	M16	G	BVRI	147	C	157.0
2007ru	S09	M16	G	UBVRI	67.6	C	69.2
2009bb	P11	M16	GH	BVRI	40	L	40.68
2010ah/PTF10bzf	M13,C11	C11	G	UVOIR <sup>g</sup>	218.8	C	228.5
2010ay	S12	M16	GH	UVOIR <sup>h</sup>	297.9	C	311.6
2012ap	M15	M16	GH	UVOIR <sup>i</sup>	43.05	L	40.37
PTF10qts	W14	M16	G	UVOIR <sup>j</sup>	415	C	428.1
PTF10vgv <sup>k</sup>	C12	M16	G	UVOIR <sup>l</sup>	60.3	C	63.5

#### Notes.

References: I00: [Iwamoto et al. \(2000\)](#); T06: [Tomita et al. \(2006\)](#); V08: [Valenti et al. \(2008\)](#); Y10: [Young et al. \(2010\)](#), S09: [Sahu et al. \(2009\)](#); P11: [Pignata et al. \(2011\)](#); M13: [Mazzali et al. \(2013\)](#); C11: [Corsi et al. \(2011\)](#); S12: [Sanders et al. \(2012\)](#); M15: [Milisavljevic et al. \(2015\)](#); W14: [Walker et al. \(2014\)](#); C12: [Corsi et al. \(2012\)](#); M16: [Modjaz et al. \(2016\)](#).

(a) None: No extinction was corrected; G: Corrected for Galactic extinction; H: Corrected for host extinction.

(b) NS: Not specified in the original paper.

(c) The distance in original paper was calculated according to the given distance modulus.

(d) L: Linear distance extracted from the NASA/IPAC Extragalactic Database (NED); C: The distance was calculated according to the latest Planck cosmological parameters.

(e) The distance adopted in this paper.

(f) The observations were available only for the *BVRI* bands. The contributions from *UV* and *IR* bands were added by assuming the same fractional contributions to the bolometric light curve as SN 2002ap.

(g) The bolometric light curve was obtained by adopting the bolometric correction from *r* band for SN 1998bw at corresponding epochs (stretched in time by  $1.3^{-1}$ ).

(h) The bolometric light curve is obtained by adopting a bolometric correction  $-0.06$  mag from *R* band.

(i) The bolometric light curve was obtained by assuming 20% contribution from the unavailable NIR band.

(j) The bolometric light curve was obtained by increasing the integrated fluxes by 15% to account for the contribution from the unavailable UV and NIR bands.

(k) [Corsi et al. \(2012\)](#) classified PTF10vgv as SN Ic based on its low Si II  $\lambda 6355$  absorption velocities, while [Modjaz et al. \(2016\)](#) reclassified it as SN Ic-BL because of its broad-lined optical spectra. Here we follow [Modjaz et al. \(2016\)](#).

(l) The bolometric light curve is obtained by adopting a bolometric correction  $-0.496$  mag from *R* band.

[jaz et al. 2016](#)). This difference may be a result of the different depth of elements in the ejecta, the degree of element mixing, and the amount of deviation from spherical expansion. Recently [Modjaz et al. \(2016\)](#) developed a comprehensive and robust way of measuring velocities for all SNe Ic-BL and SNe Ic in a self-consistent way. In this paper we use the velocity data given by [Modjaz et al. \(2016\)](#), when available. Using such a homogenous data set of velocity data reduces the bias in the resulting fitting parameters.

Usually the luminosity data of an individual SN are taken from one paper, while the data for SN 2010ah are taken from two papers (see Table 1). [Mazzali et al. \(2013\)](#) provided the bolometric luminosities for SN 2010ah up to  $\sim 70$  days, while [Corsi et al. \(2011\)](#) gave *r* band luminosities up to  $\sim 100$  days. It is found that the data from [Corsi et al. \(2011\)](#) and [Mazzali et al. \(2013\)](#) are consistent with each other within  $\pm 0.03$  mag. We converted the *r*-band luminosities given by [Corsi et al. \(2011\)](#) to bolometric luminosities according to the bolometric corrections at the nearest times given by [Mazzali et al. \(2013\)](#). In other words, the upper limit in Figure 2 of [Corsi et al. \(2011\)](#) was converted into a bolometric upper limit according to the bolometric correction of the first data point in Figure 3 of [Mazzali et al. \(2013\)](#), while the last four data points in [Corsi et al. \(2011\)](#) were modified according to the bolometric correction of the last point in [Mazzali et al. \(2013\)](#). The data given by [Corsi et al. \(2011\)](#) were also redshifted to the rest frame of this SN.

For SN PTF10vgv, only *R*-band luminosities were observed ([Corsi et al. 2012](#)). To obtain bolometric luminosities, [Corsi et al. \(2012\)](#) assumed a bolometric correction  $M_{\text{bol}} - M_R = -0.496$  mag based on the early-time photospheric temperature  $T_{\text{phot}} \approx 10^4$  K of this SN. Such a treatment is of course over-simplified because the temperature evolves rapidly during the early expansion. Another SN for which only *R*-band luminosities were observed is SN 2010ay ([Sanders et al. 2012](#)). The luminosity and expansion velocity were combined to derive a temperature of 6900 K at peak light. This implies a bolometric correction  $-0.06$  mag, according to which the bolometric luminosities are derived here. This treatment should not introduce too much bias because the observation duration of this SN is short, within 20 days before or after peak.

### 3. FITTING RESULT

As explained in [Wang et al. \(2016c,d\)](#), the model we have adopted is formulated by eight parameters. Although the model is dubbed a “magnetar model”, it also includes a  $^{56}\text{Ni}$  component. As a consequence, the model includes the usual parameters, the ejecta mass  $M_{\text{ej}}$ ,  $^{56}\text{Ni}$  mass  $M_{\text{Ni}}$ , grey optical opacity  $\kappa$ , initial expansion velocity  $v_{\text{sc0}}$ , and opacity to  $^{56}\text{Ni}$  decay photons  $\kappa_{\gamma,\text{Ni}}$ . In addition, the model includes magnetar parameters, including its dipole magnetic field  $B_p$ , initial rotation period  $P_0$  and opacity  $\kappa_{\gamma,\text{mag}}$  to account for the leakage ([Chen et al. 2015](#); [Wang et al. 2015a](#)) of high energy photons ([Murase et al. 2015](#); [Wang et al. 2016a](#)) from magne-

tars. For the grey optical opacity  $\kappa$  we take the fiducial value  $\kappa = 0.1 \text{ cm}^2 \text{ g}^{-1}$ , as used in previous investigations (Wang et al. 2016b,d). We also include the unknown explosion time  $T_{\text{start}}$  of the SN in the MCMC code. In what follows, we use the name “magnetar model” to indicate the magnetar+ $^{56}\text{Ni}$  model, except specifically mentioned otherwise.

The magnetar model proposed by Wang et al. (2016c) traces the photospheric recession and therefore the emission from the photosphere and those material outside of the photospheric radius (hereafter referred to as nebular component, or nebula for short) can be isolated. SN 2002ap is the nearest SN Ic-BL yet observed ( $D \approx 9 \text{ Mpc}$ ). Its spectra were intensely observed from very early times to late nebular stages (Foley et al. 2003; Mazali et al. 2007). An early spectrum acquired at  $\sim 81$  days past explosion shows nebular features. We examined the light curve of SN 2002ap and found that at this stage the nebula emitted about 16% of the total emission, as indicated by the vertical dotted line in Figure 1(b). If we assume that a SN begins to transition into nebular phase when the nebula radiates this percentage of emission, we can obtain the time  $T_{\text{Neb}}$  (since explosion in rest frame) by fitting the early-time light curve, as listed in Table 2.<sup>1</sup> In the magnetar model, the early peak of the light curve of a SN is caused by the spin-down of the magnetar. Consequently the  $^{56}\text{Ni}$  mass can be ignored for such early-time modeling.

Depending on the luminosity and distance, the observational qualities of the SNe are quite different. We divide the observed SNe Ic-BL light curves into two classes: those with high-quality light curves and an observational duration  $t \gtrsim 100$  days (Class I) and low-quality light curves with  $t \lesssim 100$  days (Class II). The reason for the choice of 100 days as the dividing boundary is because the lifetime of  $^{56}\text{Co}$  is  $\sim 110$  days. If observational duration is longer than 100 days, the mass of  $^{56}\text{Ni}$  can be constrained tightly. In this case we allowed the  $^{56}\text{Ni}$  mass to be a free parameter. In the opposite case, the  $^{56}\text{Ni}$  mass cannot be constrained and the only parameters that can be constrained are the magnetar parameters because it is found that in the magnetar model the early peak of the light curve can be attributed to magnetar spin-down (Wang et al. 2016b,d).

We find there are seven SNe that belong to class I, while the remaining four SNe fall in class II. Among the SNe in class I, three SNe, 1997ef, 2002ap, and 2007ru, were studied previously with our magnetar model (Wang et al. 2016b,d). SN 2002ap was investigated using an MCMC code (Wang et al. 2016d), while SNe 1997ef and 2007ru were studied via manual fitting (Wang et al. 2016b). We included them here to test the sensitivity of fitting parameters to the adoption of different photospheric velocities because the velocities used here (the values given by Modjaz et al. 2016) are different from previous studies (Wang et al. 2016b,d) where we used

<sup>1</sup> This approach is desirable as it is sometimes difficult to identify an eruption as a SN or a tidal disruption event (TDE; Brown et al. 2016; Dong et al. 2016; Leloudas et al. 2016). The indication of the early nebular phase is helpful to confirm the identity of a SN because a TDE does not have a nebular phase. We therefore encourage the modeling of the early-time light curve of a transient to give an estimate of the epoch at which nebular features may appear (if it is a SN) to help constrain the nature of the transient.

**Notes.**  
(a) Y: We determine the appearance of nebular features according to SN 2002ap; NA: Not applicable to 2002ap-p because it is a synthetic SN.  
All times in this table are in rest frame.  
In these fits, we fixed  $\kappa = 0.1 \text{ cm}^2 \text{ g}^{-1}$ .  
A hyphen indicates that this quantity cannot be constrained effectively.  
SN 2002ap-p is a synthetic SN that is 50% brighter than SN 2002ap.  
The data on the left of the vertical line are fitting parameters, while the data on the right are derived values. The MCMC code does not calculate the errors of these derived values.  
The references for the spectra are the same as in Table 1.

TABLE 2  
BEST-FITTING PARAMETERS OF OUR SNE IC-BL SAMPLE

SN	$M_{\text{ej}}$ ( $M_{\odot}$ )	$M_{\text{Ni}}$ ( $M_{\odot}$ )	$B_p$ ( $10^{15} \text{ G}$ )	$P_0$ (ms)	$v_{\text{sc0}}$ ( $\text{km s}^{-1}$ )	$\kappa_{\gamma, \text{Ni}}$ ( $\text{cm}^2 \text{ g}^{-1}$ )	$\kappa_{\gamma, \text{mag}}$ ( $\text{cm}^2 \text{ g}^{-1}$ )	$T_{\text{start}}$ (days)	$T_{\text{Neb}}$ (days)	Constraints on $T_{\text{Neb}}$ <sup>a</sup> (days)	$E_{\text{K0}}$ $10^{51} \text{ erg}$
1997ef	$3.3^{+0.21}_{-0.19}$	$0.058 \pm 0.001$	$11.4^{+0.4}_{-0.5}$	$5.2^{+1.3}_{-0.3}$	$1949^{+2577}_{-1149}$	$0.12^{+0.03}_{-0.02}$	—	$-16.1^{+0.4}_{-0.5}$	153	(61.3, 119.8)	0.07
2002ap	$2.7^{+0.11}_{-0.10}$	$0.039 \pm 0.0005$	$12.0 \pm 0.2$	$18.9 \pm 1$	$11051^{+305}_{-294}$	$0.10^{+0.003}_{-0.002}$	$4.6^{+2.3}_{-1.8}$	$1.5 \pm 0.06$	81	Y	1.97
2002ap-p	$2.7 \pm 0.11$	$0.059 \pm 0.0008$	$9.8 \pm 0.2$	$15.3 \pm 0.8$	$10978^{+312}_{-304}$	$0.10^{+0.003}_{-0.002}$	$4.6^{+2.3}_{-1.8}$	$1.5 \pm 0.06$	81	NA	1.95
2003jd	$2.45^{+0.22}_{-0.19}$	$0.081^{+0.03}_{-0.04}$	$2.29^{+0.6}_{-0.4}$	$21.5^{+0.8}_{-0.8}$	$12907^{+352}_{-307}$	$0.1^{+0.4}_{-0.3}$	$1.18^{+1.46}_{-0.87}$	$-13.7^{+0.9}_{-0.6}$	70	(62.5, 81.2)	2.43
2007bg	$1.38^{+0.15}_{-0.15}$	$0.026 \pm 0.0008$	$18.9^{+3.2}_{-3.2}$	$6.2^{+8}_{-2}$	$8337^{+3007}_{-4771}$	$1.20^{+0.3}_{-0.4}$	—	$-9.7^{+0.5}_{-0.6}$	79	(34.7, 67.7)	0.57
2007ru	$5.25 \pm 0.2$	$0.071 \pm 0.001$	$6.6 \pm 0.07$	$1.77 \pm 0.1$	$\sim 0$	$0.15 \pm 0.06$	$\gtrsim 2$	$0.06^{+0.07}_{-0.03}$	85	(70, 200)	$\sim 0$
2009bb	$1.7 \pm 0.07$	—	$2.7 \pm 0.02$	$33.0 \pm 0.2$	$13856^{+415}_{-405}$	—	—	$-11.1 \pm 0.09$	48	(55, 295)	1.90
2010ah	$2.68 \pm 1$	$0.1 \pm 0.005$	$10.3^{+1.6}_{-2.2}$	$7.0^{+10}_{-4}$	$7621^{+5186}_{-4257}$	$0.061^{+0.018}_{-0.017}$	—	$-1.2^{+0.9}_{-0.5}$	87	$> 14.5$	0.93
2010ay	$7.3^{+1.7}_{-0.9}$	—	$0.7 \pm 0.1$	$9.8^{+0.5}_{-0.9}$	$27906^{+4256}_{-4256}$	—	—	$2.3 \pm 0.4$	45	$> 44.1$	34.1
2012ap	$2.2^{+0.5}_{-0.5}$	—	$3.9^{+0.61}_{-0.38}$	$4.4^{+0.9}_{-0.4}$	$14149^{+897}_{-826}$	—	—	$0.15 \pm 0.6$	54	(38.5, 230.5)	2.62
PTF10qts	$6.5^{+4.7}_{-3.3}$	—	$2.1^{+1.7}_{-0.8}$	$20^{+5}_{-13}$	$18995^{+6950}_{-1644}$	—	—	$-19.1^{+3.8}_{-4.7}$	66	(38.8, 230.4)	13.9
PTF10xgv	$0.7^{+0.08}_{-0.07}$	$0.059 \pm 0.003$	$1.7 \pm 0.2$	$28.8^{+0.5}_{-0.7}$	$10042^{+665}_{-622}$	$0.19 \pm 0.03$	$0.013 \pm 0.001$	$6.9 \pm 0.04$	43	(46.2, 82.6)	0.42



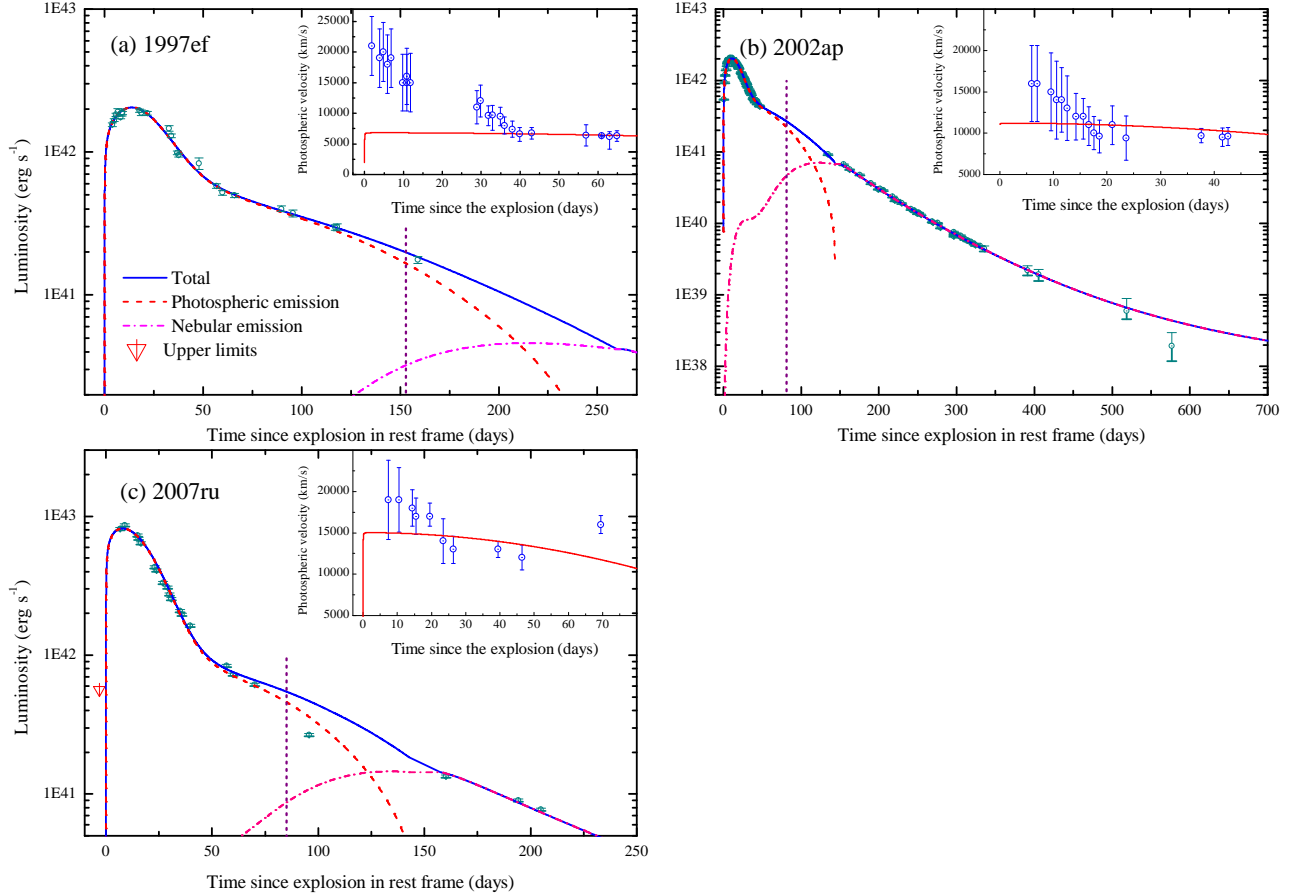


FIG. 1.— The magnetar+ $^{56}\text{Ni}$  model: best-fitting light curves (solid lines) of SNe 1997ef, 2002ap, 2007ru. The dashed and dot-dashed lines arise from photospheric and nebular emission, respectively. The vertical dotted lines mark the time when nebular emission becomes significant. The insets show the fit (red solid lines) to the evolution of photospheric velocities. For SN 2007ru, because of the small observational errors presented in Figure 2 of Sahu et al. (2009), we set the luminosity observational error to be  $\pm 0.01$  dex ( $\sim \pm 2\%$ ).

the velocities provided in the original papers. In addition, doing so will give unbiased statistical results.

The newly fitted light curves of the three previously studied SNe 1997ef, 2002ap, and 2007ru are shown in Figure 1, where emission from the photosphere and nebula are shown as dashed and dot-dashed lines, respectively. The vertical dotted lines in this figure mark the epochs when nebular emission contributes 16% of the total emission, which we assume to be the time when nebular emission features, e.g. forbidden emission lines, begin to appear. The remaining four SNe in class I are shown in Figure 2, where we show the contribution from the magnetar and  $^{56}\text{Ni}$  as dashed and dot-dashed lines, respectively. In Figure 3 the light curves were fitted with a pure magnetar model (without  $^{56}\text{Ni}$  contribution) because the  $^{56}\text{Ni}$  masses of the these four SNe in class II cannot be determined. The best-fitting values are given in Table 2. Because the contribution of magnetar and  $^{56}\text{Ni}$  to the total emission for the three SNe depicted in Figure 1 were shown previously (Wang et al. 2016b,d), we will not show them in this paper, as we do in Figure 2.

The MCMC code can only be run for those SNe for which observational errors are given. For the velocity data given by Modjaz et al. (2016), we adopted the er-

rors given in their paper. Modjaz et al. (2016) did not provide the velocity data for SN 2010ah, for which, following Wang et al. (2016d), we set the velocity errors to be half of the measured values to account for the large differences given by different velocity measurements (see e.g., Valenti et al. 2008). Most of the original papers provided luminosity errors along with luminosity data. For those SNe without luminosity errors, we have to assume a typical error for each SN. The luminosity errors of SNe 2007ru, 2007bg, 2009bb and 2012ap are given in the captions of Figures 1-3, respectively.

For some SNe, e.g. SNe 2007ru and 2007bg, the missing or sparse data coverage before peak luminosity makes the upper limits before discovery indispensable for obtaining reliable results, see Figures 1(c) and 2(b). For SN 2007ru, it is evident from Figure 1(c) that the luminosity data point at time  $\sim 95$  days cannot be fitted by our model. To obtain a reliable fitting result, this data point was omitted when we ran our MCMC code. If we failed to omit this point, the fitting result will drift to the left because the code tries to minimize the overall fitting error.

The best-fitting parameters listed in Table 2 are similar to what we found before for SNe 1997ef, 1998bw, 2002ap, and 2007ru (Wang et al. 2016b,d), where we had a de-

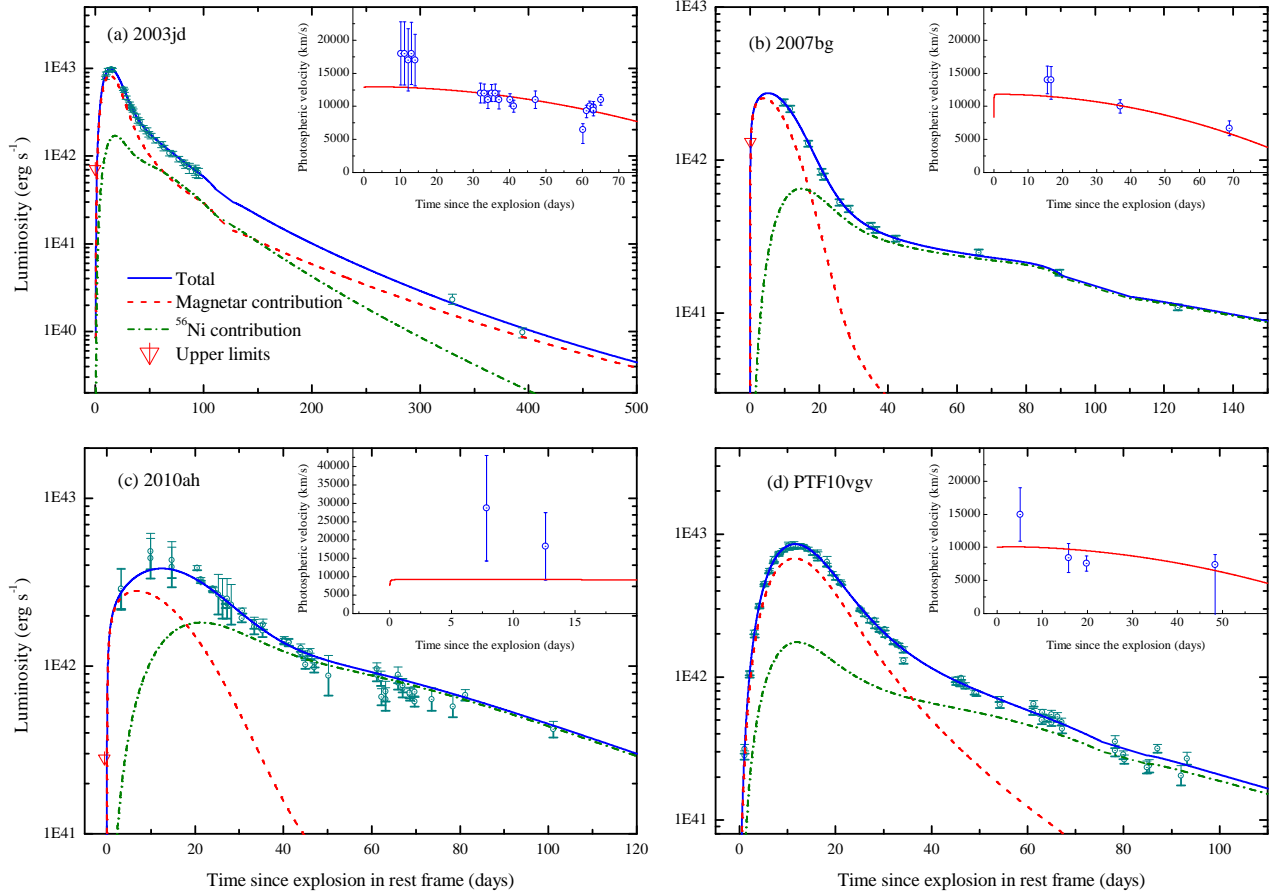


FIG. 2.— The magnetar+ $^{56}\text{Ni}$  model: best-fitting light curves (solid lines) of SNe 2003jd, 2007bg, 2010ah, and PTF10vgv. The insets show the fit (red solid lines) to the evolution of photospheric velocities. For SN 2010ah, most of the data points are taken from [Mazzali et al. \(2013\)](#), while the upper limit and the last four points are taken from [Corsi et al. \(2011\)](#). For SN 2007bg, in view of the observational errors in Figures 3 and 4 of [Young et al. \(2010\)](#), we set the luminosity error to  $\pm 0.02$  dex ( $\sim \pm 5\%$ ).

tailed discussion on the reasonability of the determined parameters such as  $M_{\text{ej}}$ ,  $M_{\text{Ni}}$ ,  $B_p$ ,  $P_0$ ,  $\kappa_{\gamma, \text{mag}}$ . We also discussed the possible reasons for a larger value of  $\kappa_{\gamma, \text{Ni}}$  than the standard value  $\sim 0.027 \text{ cm}^2 \text{ g}^{-1}$ .

From Table 2 it is evident that usually the opacity to magnetar high-energy photons  $\kappa_{\gamma, \text{mag}}$  can only be determined for SNe, i.e. 2002ap and 2003jd, observed to late stages ( $t \gtrsim 300$  days) because only at such late stages (except for the early peak) does the magnetar contribution dominate the  $^{56}\text{Ni}$  contribution. Table 2 indicates that  $\kappa_{\gamma, \text{mag}}$  is also constrained for SNe 2007ru and PTF10vgv, despite their short observation duration. For SN 2007ru the listed value of  $\kappa_{\gamma, \text{mag}}$  is favored because of the two luminosity data points at around 200 days. For PTF10vgv the given value is favored because the ejecta mass is small and high-energy radiation from the magnetar will leak, even at early stages.

Given the fitting results in Table 2, some correlations between different parameters can be examined. We show the correlations of energy versus  $^{56}\text{Ni}$  mass, energy versus ejecta mass, explosion energy versus neutron star rotational energy, energy versus dipole magnetic field of the magnetar in Figures 4–7, respectively. In the magnetar model, three forms of energy are considered here, i.e. the initial explosion energy  $E_{\text{exp}}$ , the neutron star’s

rotational energy  $E_{\text{NS}}$  and the sum of these two energies  $E_{\text{total}}$ . In the usual magnetar model that does not take into account the acceleration of the ejecta by the spinning-down magnetar, the kinetic energy of the ejecta is just the initial explosion energy. In our adopted model, the kinetic energy is no longer a constant. Instead, it evolves from its initial value, i.e. the initial explosion energy, according to the energy injection of the magnetar. The evolution of kinetic energy can be clearly appreciated by inspecting the rapid rise of the photospheric velocities at early times, e.g. SNe 1997ef, 2007ru in Figure 1 and 2007bg in Figure 2.

## 4. DISCUSSION

### 4.1. General implications

The high fitting quality both for luminosities and velocities can be appreciated from Figures 1–3. The only exception may be the velocity fitting result of SN 1997ef and the luminosity fitting result of SN 2009bb. For SN 1997ef, and to a less extent, SN 2003jd, and SN 2009bb, the early-time velocities cannot be fitted. A possible way of getting better fitting results may be the introduction of a fast-moving shell in the ejecta. This hypothesis is also supported by the earlier appearance of nebular spectrum than our prediction, see Section 4.2. For SN 2009bb

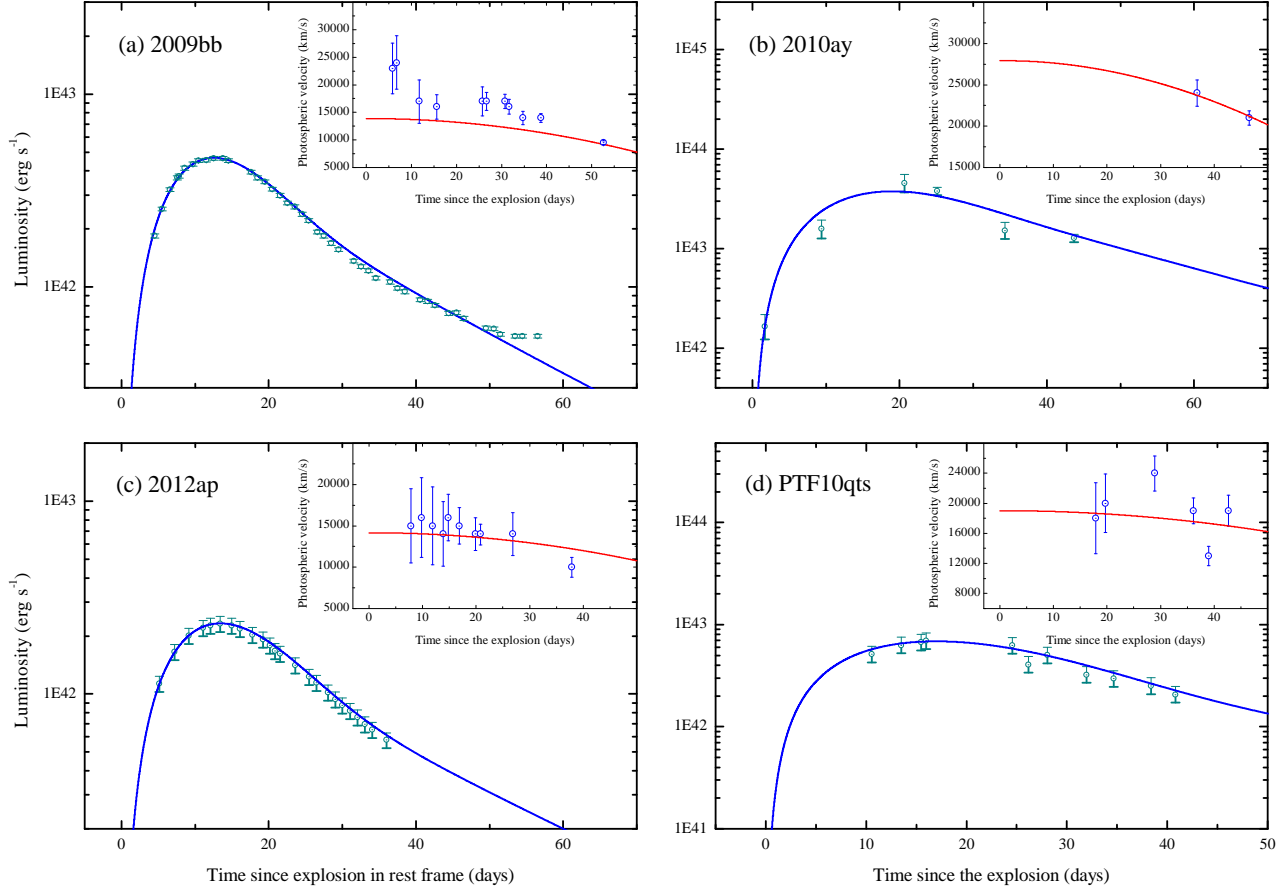


FIG. 3.— Light curves of SNe 2009bb, 2010ay, 2012ap, PTF10qts fitted by a pure-magnetar (without  $^{56}\text{Ni}$ ) model. The insets show the fit (red solid lines) to the evolution of photospheric velocities. The luminosity observational errors for SNe 2009bb and 2012ap were set to  $\pm 0.01$  dex ( $\sim \pm 2\%$ ) and  $\pm 0.04$  dex ( $\sim \pm 10\%$ ), respectively.

it seems necessary to include a contribution of  $^{56}\text{Ni}$ , as indicated by the much improved fitting result in Figure 8.

We have examined the effect of adopting different velocity data on the derived parameters. It turns out that the values of  $M_{\text{Ni}}$ ,  $B_p$ ,  $\kappa_{\gamma, \text{Ni}}$ ,  $\kappa_{\gamma, \text{mag}}$ , and  $T_{\text{start}}$  are insensitive to the expansion velocity, while  $M_{\text{ej}}$ ,  $P_0$ , and  $v_{\text{sc0}}$  are sensitive to the expansion velocity. This is because the former group of parameters are determined by the light curve shape, while the latter group of parameters mainly affect the dynamics of the ejecta.

From Table 2 it is evident that in the magnetar (plus  $^{56}\text{Ni}$ ) model, the initial SN explosion energies are usually smaller than  $\sim 2.5 \times 10^{51}$  erg, i.e. the theoretical upper limit of explosion energy triggered by neutrino heating (Janka et al. 2016). There are two exceptions, SNe 2010ay and PTF10qts, which have explosion energies  $\gtrsim 10^{52}$  erg. We note that the light curves of these two SNe are poorly sampled and it is possible to attribute a fraction of the energy to magnetar by tuning up the rotational energy of the magnetar. We conclude that the explosion energy of all well-observed SNe can be explained by neutrino heating.

As mentioned in Section 2, determination of the bolometric luminosity usually suffers from significant uncertainties. To evaluate the effects of such uncertainties

on the derived parameters, we artificially shifted the luminosities of SN 2002ap upwards by 50%, but kept the velocities unchanged. We choose SN 2002ap because it is the best observed SN in our sample and all of the fitting parameters can be determined accurately. We list the shifted SN 2002ap as SN 2002ap-p in Table 2. It can be seen that the only affected parameters are  $M_{\text{Ni}}$ ,  $B_p$ ,  $P_0$ .

This experiment also shows that the mass of  $^{56}\text{Ni}$  is directly proportional to the luminosity in the exponential decay phase, that is,  $M_{\text{Ni}}$  is shifted upwards by 50% (see Table 2). This is particularly interesting when we look at the  $^{56}\text{Ni}$  mass of SN 2007bg, which harbours the lowest amount of  $^{56}\text{Ni}$  within the sample. The actual  $^{56}\text{Ni}$  mass of SN 2007bg should be higher because its light curve was integrated only over the optical bands. If we shift the light curve of SN 2007bg by 50% upwards (the  $IR$  contribution can be as significant as 30% or more at the exponential decay phase, see Cano et al. 2011), the derived  $^{56}\text{Ni}$  mass will be the same as that of SN 2002ap. This shows that the  $^{56}\text{Ni}$  masses in this sample of SNe Ic-BL, for which the  $^{56}\text{Ni}$  mass can be constrained, lie in a narrow range,  $0.04 - 0.1 M_{\odot}$ .

Table 2 shows that the initial explosion energy of the synthetic SN 2002ap-p is slightly lower than SN 2002ap. This is because a brighter SN needs a magnetar spinning faster, and therefore more rotational energy is available

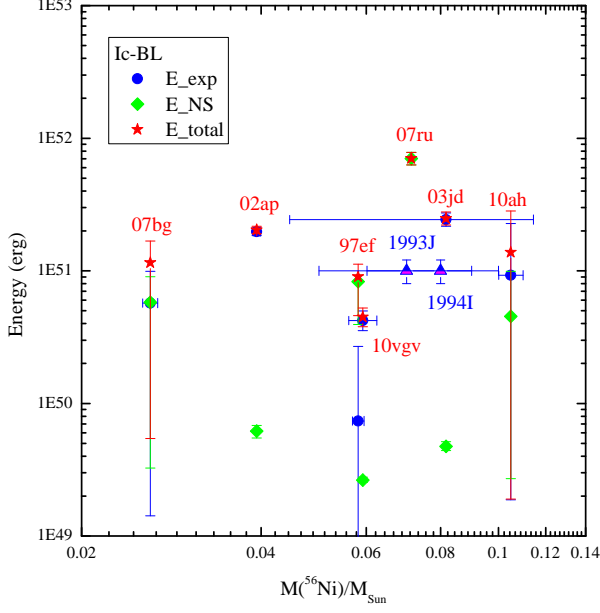


FIG. 4.—  $^{56}\text{Ni}$  mass versus explosion energy, neutron star rotational energy, and the sum of these two energies. The ordinary SNe 1993J (Iib) and 1994I (Ic) are plotted as triangles. For clarity, only one  $^{56}\text{Ni}$  error bar is shown for each SN.

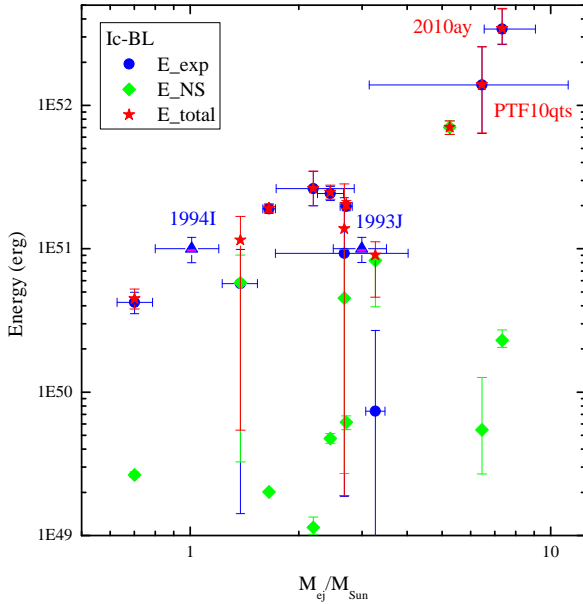


FIG. 5.— Ejecta mass versus explosion energy, neutron star rotational energy, and the sum of these two energies. The ordinary SNe 1993J (Iib) and 1994I (Ic) are plotted as triangles. For clarity, only one ejecta mass error bar is shown for each SN.

to accelerate the ejecta, reducing the required initial explosion energy. It should be mentioned that  $M_{\text{ej}}$  is not affected by such shift. Although the uncertainties of a real SN cannot be so simplified, such an experiment serves as a guide for estimating the reliability of the fitting parameters.

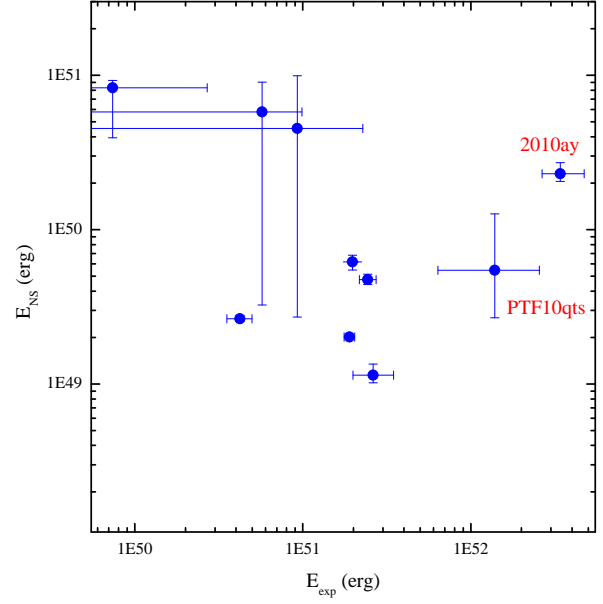


FIG. 6.— Explosion energy versus neutron star rotational energy.

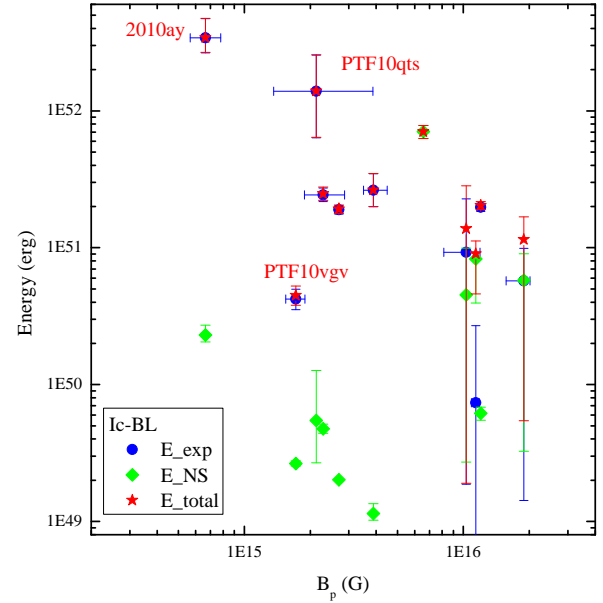


FIG. 7.—  $B_p$  versus explosion energy, neutron star rotational energy, and the sum of these two energies. For clarity, only one  $B_p$  error bar is shown for each SN.

Table 2 shows that the fitting parameters of the two relativistic SNe, 2009bb and 2012ap, are typical among this SNe Ic-BL sample. It is therefore unlikely to acquire more clue on the explosion mechanism of relativistic SNe solely from such fitting parameters, if the magnetar model is the right model for such SNe. A thorough comparison between SNe Ic-BL and those associated with GRBs is required to get more clue.

PTF10vgv is peculiar because of its low absorption ve-



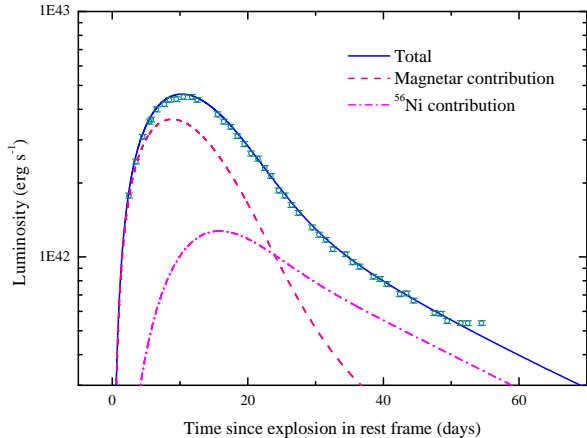


FIG. 8.— Light curve of SN 2009bb that includes a contribution of  $^{56}\text{Ni}$ .

locities (typical of ordinary SNe Ic) and broad-lined optical spectra (typical of SNe Ic-BL). It has the lowest ejecta mass,  $0.7M_{\odot}$ , in the SNe Ic-BL sample (see Table 2). Its opacity to magnetar photons,  $\kappa_{\gamma, \text{mag}} = 0.013 \text{ cm}^2 \text{ g}^{-1}$ , is also much lower than the values found for the other SNe Ic-BL. Corsi et al. (2012) constrained its progenitor radius to be  $R < (1 - 5) R_{\odot}$ , consistent with a compact Wolf-Rayet star. These peculiarities may indicate that PTF10vgv lies in the gap between SNe Ic and SNe Ic-BL.

The MCMC code can determine the explosion time accurately if the light-curve data are of high quality. The most excellent case is SN 1998bw, for which the explosion time was constrained to be  $-0.009^{+0.32}_{-0.36}$  days relative to the GRB trigger time (Wang et al. 2016d). In Table 3 we compare the explosion time determined in this work with those given in the literature. Also listed in this table are the discovery date and date of non-detection. The explosion time is computed according to the times  $T_{\text{start}}$  given in Table 2, after correcting for cosmological time dilation.

In the calculation of the explosion time, we frequently need the time of V-band maximum, which we consult Modjaz et al. (2014). Because the explosion time determined in this work is calculated according to the relevant time given in the original paper, the uncertainties of the explosion time are the errors given in the original paper, if available, or the errors of  $T_{\text{start}}$  given in Table 2, whichever is larger.

It can be seen from Table 3 that the times determined in this work are generally in good agreement with those given in the literature. The only exception is SN 1997ef, for which our determination, which is almost coincident with the discovery date, is  $\sim 5$  days later than that given by Mazzali et al. (2000). Please note that the first bolometric data point in Figure 1 is 4 days later than the discovery date. For PTF10qts, the theoretical light curve is below the non-detection upper limit on August 2, 2010. Because of the poor quality of its light curve, the uncertainty of the explosion date of PTF10qts is large. See Section 4.4 for more discussion on the determination of explosion time.

#### 4.2. Estimate the appearance of nebular features from early light curve modeling

In this paper we propose to calculate the time  $T_{\text{Neb}}$  when the nebular features begin to emerge in the SN spectra, based on the well-observed SN 2002ap. It is desirable to compare this time with observations of other SNe. We searched the spectra from the references listed in Table 1. The lower limit of  $T_{\text{Neb}}$  for a SN in question is the latest time at which a spectrum is photospheric, while the upper limit is the earliest time at which the spectrum is nebular. We list these constraints in Table 2.

The spectrum taken on 26 January, 1998 of SN 1997ef is photospheric (Mazzali et al. 2000), while the first nebular spectrum is on +104 days (in rest frame) post  $R$ -band maximum (Young et al. 2010), implying the transition from photospheric to nebular occurred between these two dates. Next, the spectrum obtained +51 days post  $B$ -band maximum of SN 2003jd is photospheric, while the spectrum on +70 days is nebular (Valenti et al. 2008). For SN 2007bg, the spectrum taken at +25 days post  $R$ -band maximum for SN 2007bg is photospheric, while the spectrum on +58 days is nebular (Young et al. 2010). For SN 2007ru, the spectrum obtained 70 days after explosion for SN 2007ru is photospheric, while the spectrum on 200 days is nebular (Sahu et al. 2009). Next, the spectrum of SN 2009bb on +45 days past  $B$ -band maximum is photospheric, while the spectrum on +285 days is nebular (Pignata et al. 2011). For SN 2012ap, the spectrum taken at +26 days past  $B$ -band maximum is photospheric, while the spectrum on +218 days is nebular (Milisavljevic et al. 2015). For PTF10qts, the spectrum taken +21 days past  $R$ -band maximum is photospheric, while the spectrum on +230 days is nebular (Walker et al. 2014). Finally, for PTF10vgv the spectrum obtained at +35 days past  $R$ -band maximum is photospheric, while the spectrum on +72 days is nebular (Corsi et al. 2012).

For SN 2010ah, the spectrum of SN 2010ah on 7, March, 2010 is photospheric (Mazzali et al. 2013), with no data later than this date being published. The same situation applies for SN 2010ay, of which that latest spectrum was obtained on +24 days past  $R$ -band maximum is photospheric (Sanders et al. 2012). For both of these events, the precise timing of the transition from the photospheric phase to the nebular can only be constrained to have occurred after these dates.

We can see from Table 2 that our fitting constraints of  $T_{\text{Neb}}$  for SNe 2002ap, 2003jd, 2007ru, 2010ah, 2010ay, 2012ap, and PTF10qts are consistent with observations. For PTF10vgv,  $T_{\text{Neb}}$  (43 days) is slightly earlier than the lower limit 46.2 days. For SN 2009bb the given  $T_{\text{Neb}}$  (48 days) is 7 days earlier than observation. This may be caused by the helium envelope of this SN because early-time optical spectra showed evidence for the presence of helium in this SN (Pignata et al. 2011; another SN that evidenced with some helium is SN 2012ap, Milisavljevic et al. 2015). The helium envelope will delay the appearance of nebular lines. For SN 2007bg,  $T_{\text{Neb}}$  (79 days) is 11 days later than the upper limit. This large discrepancy for SN 2007bg might be caused by the sparsity of data before peak time, see Figure 2(b).

For 1997ef,  $T_{\text{Neb}}$  (153 days) is significantly later than the appearance of the first nebular spectrum, i.e.

TABLE 3  
COMPARISON OF EXPLOSION TIMES DERIVED IN THIS WORK AND PREVIOUS PAPERS.

SN	This work	Previous estimate	Discovery date	Date of non-detection	References
1997ef	1997/11/25 $^{+0.4}_{-0.5}$	1997/11/20	1997/11/25	1997/11/16	H97,M00
2002ap	2002/01/27 $\pm 0.5$	2002/01/25.5 $\pm 0.5$	2002/01/29	2002/01/25	M02,T06
2003jd	2003/10/16.8 $^{+0.9}_{-1}$	<2003/10/17	2003/10/25	2003/10/16	V08
2007bg	2007/04/06 $^{+0.5}_{-0.6}$	—	2007/04/16.15	2007/04/06	Y10
2007ru	2007/11/25.5 $^{+0.07}_{-0.03}$	2007/11/25.5	2007/11/27.9	2007/11/22	S09
2009bb	2009/03/19.3 $\pm 0.6$	2009/03/19.1 $\pm 0.6$	2009/03/21.11	2009/03/19.2	P11
2010ah	2010/02/19.7 $^{+0.9}_{-0.5}$	2010/02/17.8–2010/02/23.5	2010/02/23.5	2010/02/19.4	C11
2010ay	2010/02/22.96 $\pm 1.3$	2010/02/21.3 $\pm 1.3$	2010/03/05.45	2010/02/17.45	S12
2012ap	2012/02/05 $\pm 2$	2012/02/05 $\pm 2$	2012/02/10.23	—	M15
PTF10qts	2010/07/26.25 $^{+3.8}_{-4.7}$	—	2010/08/05.23	2010/08/02	W14
PTF10vgv	2010/9/13.2 $\pm 0.04$	—	2010/09/14.1	2010/09/12.5	C12

#### Notes.

UT dates are used in this table.

A hyphen indicates that the date was not specified in the original paper.

References: H97: [Hu et al. \(1997\)](#); M00: [Mazzali et al. \(2000\)](#); M02: [Mazzali et al. \(2002\)](#); T06: [Tomita et al. \(2006\)](#); V08: [Valenti et al. \(2008\)](#); S09: [Sahu et al. \(2009\)](#); Y10: [Young et al. \(2010\)](#); C11: [Corsi et al. \(2011\)](#); P11: [Pignata et al. \(2011\)](#); C12: [Corsi et al. \(2012\)](#); S12: [Sanders et al. \(2012\)](#); W14: [Walker et al. \(2014\)](#); M15: [Milisavljevic et al. \(2015\)](#);

119.8 days. As we mentioned in Section 4.1, a plausible reason for this large discrepancy may lie in the failure of our model to fit the early velocity data. We suggest that a fast-moving shell should be introduced for SN 1997ef. Such a shell will contribute a significant fraction of nebular emission and therefore made the appearance of nebular phase earlier.

In summary, we conclude that  $T_{\text{Neb}}$  determined in this way is in general a good guide for the emergence of nebular features, although it is not completely accurate. Other factors come into play in determining the emergence of nebular lines aside from the amount of nebular emission.

#### 4.3. Correlations

In the magnetar model, the required  $^{56}\text{Ni}$  mass is, unsurprisingly, reduced significantly. It is therefore expected that the  $^{56}\text{Ni}$  mass-energy relation will be quite different, as depicted in Figure 4, where we also plot the ordinary type IIb SN 1993J and type Ic SN 1994I. It is clear from this figure that the synthesized  $^{56}\text{Ni}$  is consistent with ordinary SNe. There is no clear increase of  $^{56}\text{Ni}$  mass with increased energy, contrary to earlier findings ([Mazzali et al. 2013](#)). In the magnetar model, the explosion energies are generally significantly lower than in pure- $^{56}\text{Ni}$  models, regardless whether it is the one-dimensional  $^{56}\text{Ni}$  model or two-component  $^{56}\text{Ni}$  model. The explosion energy is no longer the sole decisive factor for  $^{56}\text{Ni}$  synthesis. In this case the synthesis of  $^{56}\text{Ni}$  may be determined by other factors, e.g. the radius, and/or density profile of the progenitor star ([Smartt 2009](#)). Such diversity may reflect the mass, binarity, metallicity, mass-loss rate, rotation, and magnetic field of the main sequence star ([Smartt 2009](#)).

Table 2 shows that the explosion energy of SN 2007ru is quite low, but the  $^{56}\text{Ni}$  mass  $M_{\text{Ni}}$  is not zero. This indicates that the  $^{56}\text{Ni}$  of this SN was synthesized by the shock wave generated by the spinning-down magnetar ([Nishimura et al. 2015](#); [Suwa & Tominaga 2015](#)). This is in agreement with expectations because the rotational energy of the magnetar powering SN 2007ru is the largest in the SNe Ic-BL sample. The magnetic field

$B_p$  is also strong enough to synthesize the needed  $^{56}\text{Ni}$ . In the magnetar model, both the explosion shock and the magnetar-powered shock can synthesize  $^{56}\text{Ni}$ . This complicates the  $^{56}\text{Ni}$  mass-energy relation of SNe Ic-BL.

From Figure 5 it is clear that the ejecta mass increases with energy. This is similar to earlier findings ([Mazzali et al. 2013](#)), but the energies are much smaller than the values given by pure- $^{56}\text{Ni}$  models ([Mazzali et al. 2013](#)).

We also examined the relation between explosion energy and neutron star rotational energy, given in Figure 6. This figure seems to indicate that there is no clear correlation between these two energies. However, if we consider that the fitting parameters of SNe 2010ay and PTF10qts are not very reliable, as discussed above, and hence remove them from this discussion, the figure seems to suggest an anti-correlation between these two energies (correlation coefficient is 0.49). If this is true, it may indicate that for SNe Ic-BL the explosion energy and neutron star rotational energy come from the same energy reservoir, e.g. the pre-explosion rotational energy of the progenitor.

Figure 7 seems to imply a rough anti-correlation between magnetic field  $B_p$  and energy. However, if the two exceptional SNe, 2010ay and PTF10qts, are eliminated from this figure, no clear correlation is seen between these two quantities. Because  $B_p$  harbours a fraction of the toroidal magnetic field within the neutron star,  $B_p$  can serve as an indication of the magnetic energy present within the neutron star. If this is true, Figure 7 may imply that the amplification of magnetic field in the neutron star is unrelated with the explosion energy.

#### 4.4. Alternative models?

In this paper we tested the hypothesis that all SNe Ic-BL are powered by a combination of input from a magnetar central engine and  $^{56}\text{Ni}$  synthesized during the initial explosion. Next, we ask the question that can a pure- $^{56}\text{Ni}$  model or a pure-magnetar model give comparable results? It is well known that the one-dimensional  $^{56}\text{Ni}$  model cannot give a satisfactory description for SNe with long observation durations ([Iwamoto et al. 2000](#); [Nakamura et al. 2001](#); [Maeda et al. 2003](#)). As a result the

two-component model was employed to investigate most of the SNe in Figures 1 and 2 (SNe 1997ef, 2002ap, Maeda et al. 2003; SN 2003jd, Valenti et al. 2008; SN 2007bg, Young et al. 2010).

We will not examine these SNe within the framework of two-component model because the SNe in Figures 1 and 2 have comparable peak luminosities. We will instead test the two-component model with the four SNe in Figure 3 and compare the results with the parameters determined using a pure-magnetar model in Table 2. SN 2010ay in this figure is particularly interesting because its peak luminosity  $\sim 4.5 \times 10^{43} \text{ erg s}^{-1}$  is comparable to some of the SLSNe, PTF10hgi ( $3.52 \times 10^{43} \text{ erg s}^{-1}$ ; Inserra et al. 2013), PTF11rks ( $4.7 \times 10^{43} \text{ erg s}^{-1}$ ; Inserra et al. 2013), and PS1-14bj ( $4.6 \times 10^{43} \text{ erg s}^{-1}$ ; Lunnan et al. 2016), see also Table 1 in Liu et al. (2017). Such SLSNe are usually assumed to be powered by magnetars because of the failure of  $^{56}\text{Ni}$  model.

In Table 4 we list the best-fitting parameters of SNe 2009bb, 2010ay, 2012ap, and PTF10qts using the pure- $^{56}\text{Ni}$  model along with a comparison of  $\chi^2/(\text{degree of freedom})$  obtained using the pure- $^{56}\text{Ni}$  model and pure-magnetar model. Because the fitting quality of the pure- $^{56}\text{Ni}$  model for these four SNe are comparable to that of the pure-magnetar model, we do not show the light-curve fitting results of the pure- $^{56}\text{Ni}$  model for these SNe.

As expected, the best-fitting parameters for SNe 2009bb, 2012ap, and PTF10qts are reasonable, while the parameters for SN 2010ay are in tension with a typical CCSN. The ratio of  $^{56}\text{Ni}$  mass to the ejecta mass is 0.27, which is larger than the upper limits 0.2 expected for a CCSN (Umeda & Nomoto 2008). More problematically, the needed  $^{56}\text{Ni}$  mass  $1.9M_{\odot}$ <sup>2</sup> is somewhat incompatible with a CCSN but in accordance with a pair instability SN (PISN; Barkat et al. 1967; Rakavy & Shaviv 1967). Its ejecta mass is, however, not expected for a PISN. We therefore conclude that SN 2010ay is unlikely to be explained by a pure- $^{56}\text{Ni}$  model, including the two-component model.

For PTF10qts, Walker et al. (2014) obtained  $M_{\text{Ni}} = 0.35 \pm 0.1M_{\odot}$ , based on a model fit to the nebular spectrum of this SN. Such an estimate of  $^{56}\text{Ni}$  mass is consistent with the value given in Table 4 in the pure- $^{56}\text{Ni}$  model. This seems to argue against our hypothesis that all SNe Ic-BL were powered by magnetars. However, on the one hand, as commented by Walker et al. (2014), any firm conclusions should not be drawn based on this result because of the low signal-to-noise ratio of the observed spectrum. On the other hand, for any SN Ic-BL with a long observational duration, some amount of  $^{56}\text{Ni}$  is indeed required, although its amount is significantly lower than in the pure- $^{56}\text{Ni}$  model.

For those SNe whose  $M_{\text{Ni}}$  can be constrained, the small errors associated with  $M_{\text{Ni}}$ , as presented in Table 2, clearly indicate the necessity of including  $^{56}\text{Ni}$  to give the best-fitting results. The synthesis of  $^{56}\text{Ni}$  is also expected in a CCSN. Neglecting  $M_{\text{Ni}}$  will usually result in rather poor fitting quality, as shown in Figure 9 with the

best-fitting parameters listed in Table 5. In Figure 9 we do not show the fitting result of SN 2007bg because the rapid rise and decline around peak require unreasonable parameters ( $v_{\text{sc0}} = 143109^{+12052}_{-10316} \text{ km s}^{-1}$ ), as shown in Table 5, in spite of fair fitting quality of the light curve. In Table 5 we also compare the reduced  $\chi^2$  of the pure-magnetar model and magnetar+ $^{56}\text{Ni}$  model.

The high fitting quality of the magnetar+ $^{56}\text{Ni}$  model can be most easily appreciated by comparing the reproduced light curves of SN 2002ap by these two models. The ejecta masses given by the pure-magnetar model are frequently unreasonable, e.g. SN 2002ap and PTF10vgv. For SN 1997ef, the magnetar+ $^{56}\text{Ni}$  model is favored not only because of the smaller reduced  $\chi^2$  compared to the pure-magnetar model, but also because of the broad peak of this SN, as found by Iwamoto et al. (2000). Comparing Figures 1(a) and 9(a) indicates that the magnetar+ $^{56}\text{Ni}$  model captures the broad peak of this light curve better than the pure-magnetar model, see Figure 1 in Wang et al. (2016b) for a clearer rendering. For SNe 2003jd, 2007ru, and 2010ah, the contribution of  $^{56}\text{Ni}$  is not necessary to give an acceptable fitting result.

To fit the light curves by the pure-magnetar model, the velocity fitting results are frequently bad, e.g. SNe 2002ap and PTF10vgv (see Figure 9), besides the above mentioned SN 2007bg. The low velocities are required for these SNe in the pure-magnetar model because of the slow decline rates of the light curves.

The above results indicate that the magnetar+ $^{56}\text{Ni}$  model is the best model in reproducing the light curves and velocity evolutions of the SNe Ic-BL sample, although some SNe can also be well described by the two-component  $^{56}\text{Ni}$  model (e.g., SNe 1997ef, 2002ap), while some others (e.g., SNe 2003jd, 2007ru, and 2010ah) can also be well reproduced by the pure-magnetar model.

We note that different models usually give different explosion times, as can be found by comparing  $T_{\text{start}}$  presented in Tables 2, 4, and 5. Tables 2 and 5 show that the explosion times determined by the magnetar+ $^{56}\text{Ni}$  model are all later than that determined by the pure-magnetar model, with PTF10vgv the only exception. This can be well understood. To account for the late-time light curves, the spin-down timescales of the magnetars in the pure-magnetar model have to be longer than in the magnetar+ $^{56}\text{Ni}$  model. This will result in slow rise rate and therefore the explosion times must be somewhat earlier. The slow rise rates in the pure-magnetar model suffer from some tension with the upper limits of the light curves of SNe 2003jd, 2007ru, 2010ah, as can be seen from Figure 9.

Comparison of  $T_{\text{start}}$  in Tables 2 and 4 shows that the explosion times in the magnetar+ $^{56}\text{Ni}$  model are usually later than that in the  $^{56}\text{Ni}$  model, except for SN 2010ay. This can be understood by comparing the spin-down timescale of the magnetar,  $\tau_{\text{sd}}$ , with the  $^{56}\text{Ni}$  decay timescale,  $\tau_{\text{Ni}} = 8.8 \text{ days}$ . It is found that  $\tau_{\text{sd}} = 8.0, 11.5, 6.8, 4.7 \text{ days}$  for SNe 2009bb, 2010ay, 2012ap, PTF10qts, respectively. If  $\tau_{\text{sd}} < \tau_{\text{Ni}}$ , the energy of the magnetar is released more rapidly in the magnetar model than in the  $^{56}\text{Ni}$  model, the rise time in the magnetar model is shorter than in the  $^{56}\text{Ni}$  model. This is why the explosion time of SN 2010ay in the magnetar model is earlier than in the  $^{56}\text{Ni}$  model because in this case  $\tau_{\text{sd}} > \tau_{\text{Ni}}$ .

<sup>2</sup> Wang et al. (2015b) found that  $M_{\text{Ni}} = 2M_{\odot}$  is required to meet the peak luminosity of SN 2010ay for a  $^{56}\text{Ni}$  model. This indicates that Sanders et al. (2012) underestimated the  $^{56}\text{Ni}$  mass of SN 2010ay.

TABLE 4  
BEST-FITTING PARAMETERS FOR THE SNE IN FIGURE 3 USING THE PURE- $^{56}\text{Ni}$  MODEL

SN	$M_{\text{ej}}$ ( $M_{\odot}$ )	$M_{\text{Ni}}$ ( $M_{\odot}$ )	$v_{\text{sc0}}$ ( $\text{km s}^{-1}$ )	$T_{\text{start}}$ (days)	$\chi^2/\mu$	
					pure- $^{56}\text{Ni}$ model	magnetar model
2009bb	$1.5 \pm 0.08$	$0.17 \pm 0.001$	$15760^{+450}_{-430}$	$-12.3 \pm 0.12$	3.22	1.88
2010ay	$7^{+0.6}_{-0.5}$	$1.9 \pm 0.1$	$29293^{+1815}_{-1612}$	$2.0^{+0.3}_{-0.4}$	1.0	1.68
2012ap	$1.4^{+0.15}_{-0.14}$	$0.086 \pm 0.0018$	$15097^{+771}_{-769}$	$-0.45^{+0.43}_{-0.48}$	0.044	0.085
PTF10qts	$3.8^{+1}_{-0.8}$	$0.3^{+0.03}_{-0.02}$	$21121^{+1313}_{-1244}$	$-20.4^{+2.8}_{-3.8}$	0.75	0.78

**Notes.** In these fits, we fixed  $\kappa = 0.1 \text{ cm}^2 \text{ g}^{-1}$ ,  $\kappa_{\gamma, \text{Ni}} = 0.027 \text{ cm}^2 \text{ g}^{-1}$ .

TABLE 5  
BEST-FITTING PARAMETERS OF THE SNE IN FIGURES 1 AND 2 USING THE PURE-MAGNETAR MODEL

SN	$M_{\text{ej}}$ ( $M_{\odot}$ )	$B_p$ ( $10^{15} \text{ G}$ )	$P_0$ (ms)	$v_{\text{sc0}}$ ( $\text{km s}^{-1}$ )	$\kappa_{\gamma, \text{mag}}$ ( $\text{cm}^2 \text{ g}^{-1}$ )	$T_{\text{start}}$ (days)	$\chi^2/\mu$	
							pure-magnetar	magnetar+ $^{56}\text{Ni}$
1997ef	$1.8 \pm 0.08$	$1.5 \pm 0.02$	$37.4 \pm 0.2$	$7674^{+149}_{-150}$	$\gtrsim 3$	$-25.5^{+0.4}_{-0.3}$	2.25	1.51
2002ap	$0.62^{+0.05}_{-0.04}$	$2.5 \pm 0.016$	$46.8 \pm 0.1$	$6525^{+404}_{-401}$	$0.4 \pm 0.03$	$-1.9^{+0.08}_{-0.09}$	6.16	0.96
2003jd	$2.3 \pm 0.14$	$1.5 \pm 0.03$	$21.1 \pm 0.3$	$13510^{+448}_{-449}$	$0.66^{+0.11}_{-0.09}$	$-15.5^{+0.6}_{-0.5}$	0.4	0.3
2007bg	$8.7^{+2.1}_{-1.8}$	$1.4^{+0.12}_{-0.15}$	$51.9^{+1.3}_{-1.9}$	$143109^{+12052}_{-10316}$	$13.2^{+27}_{-5.8}$	$-13^{+1.3}_{-1.4}$	8.36	0.32
2007ru	$2.7 \pm 0.13$	$1.9 \pm 0.01$	$22 \pm 0.15$	$14037^{+543}_{-538}$	$\gtrsim 5$	$-4.7 \pm 0.1$	3.3	3.7
2010ah	$0.98^{+0.36}_{-0.30}$	$1.7^{+0.05}_{-0.07}$	$31.2 \pm 0.3$	$10659^{+2444}_{-2681}$	$\gtrsim 8$	$-3.2^{+0.4}_{-0.3}$	0.8	0.8
PTF10vgv	$0.29^{+0.008}_{-0.007}$	$2.4^{+0.016}_{-0.014}$	$24 \pm 0.2$	$\sim 0$	$4.2^{+2.5}_{-2.7}$	$6.9^{+0.04}_{-0.03}$	1.2	0.7

**Notes.** In these fits, we fixed  $\kappa = 0.1 \text{ cm}^2 \text{ g}^{-1}$ .

By this way, it is not difficult to understand why the explosion time of SN 1997ef is almost coincident with the discovery date in the magnetar+ $^{56}\text{Ni}$  model. From Table 2 it is found that  $\tau_{\text{sd}} = 0.01$  days for this SN. The energy was almost explosively released.

## 5. CONCLUSIONS

The mechanism for the formation of SNe Ic-BL is still unclear. Recently there is strong evidence that SNe Ic-BL are powered by magnetars (Wang et al. 2016d). Indeed, for all of the SNe Ic-BL that were observed to phases  $\gtrsim 300$  days when the contribution from  $^{56}\text{Ni}$  decays significantly, there is clear evidence for magnetar formation.

Motivated by this evidence, we studied a sample of  $N = 11$  SNe Ic-BL and obtain their light curve fitting parameters. From this study it is evident that the sample of SNe Ic-BL can be reasonably described by our magnetar model. The magnetar model naturally reduces the needed  $^{56}\text{Ni}$  and simultaneously accounts for the origin of the huge kinetic energies observed in SNe Ic-BL, with only two exceptions, SNe 2010ay and PTF10qts, which could be attributed to the poor quality of the light curves. We also examine the possibility for the pure- $^{56}\text{Ni}$

or pure-magnetar model to explain the light curve and velocity evolution. It is found that SN 2010ay is in tension with the  $^{56}\text{Ni}$  model, while SNe 2003jd, 2007ru, and 2010ah are compatible with the pure-magnetar model.

Our results indicate that the synthesized  $^{56}\text{Ni}$  mass does not increase with explosion energy or neutron star rotational energy. The  $^{56}\text{Ni}$  mass is consistent with ordinary SNe. The relation between explosion energy and neutron star rotational energy seems to imply a common energy reservoir for these two energies. It seems to indicate that the amplification of magnetic field of the neutron star is independent of the explosion energy. To get a more robust statistical result, more observations are definitely needed.

We thank Maryam Modjaz and Yuqian Liu for sending us the photospheric velocity data before the publication of their paper. This work is supported by the National Basic Research Program (“973” Program) of China under Grant No. 2014CB845800 and the National Natural Science Foundation of China (grant Nos. U1331202, 11533033, U1331101, 11573014, 11422325 and 11373022.). D.X. acknowledges the support of the One-Hundred-Talent Program from the National Astronomical Observatories, Chinese Academy of Sciences.

## REFERENCES

- Ade, P. A. R., Aghanim, N., Arnaud, M., et al. 2016, *A&A*, 594, A13
- Barkat, Z., Rakavy, G., & Sack, N. 1967, *PhRvL*, 18, 379
- Bietenholz, M. F., Soderberg, A. M., Bartel, N., et al. 2010, *ApJ*, 725, 4
- Brown, P. J., Yang, Y., Cooke, J., et al. 2016, *ApJ*, 828, 3
- Cano, Z., Bersier, D., Guidorzi, C., et al. 2011, *ApJ*, 740, 41
- Cano, Z., de Ugarte Postigo, A., Perley, D., et al. 2015, *MNRAS*, 452, 1535
- Cano, Z., Jakobsson Andreas, K. G., & Geirsson, O. P. 2014, arXiv:1409.3570
- Cano, Z., Johansson Andreas, K. G., & Maeda, K. 2016a, *MNRAS*, 457, 2761
- Cano, Z., Wang, S. Q., Dai, Z. G., & Wu, X. F. 2016b, arXiv:1604.03549
- Chakraborti, S., Ray, A., Soderberg, A. M., Loeb, A., & Chandra, P. 2011, *NatCo*, 2, 175



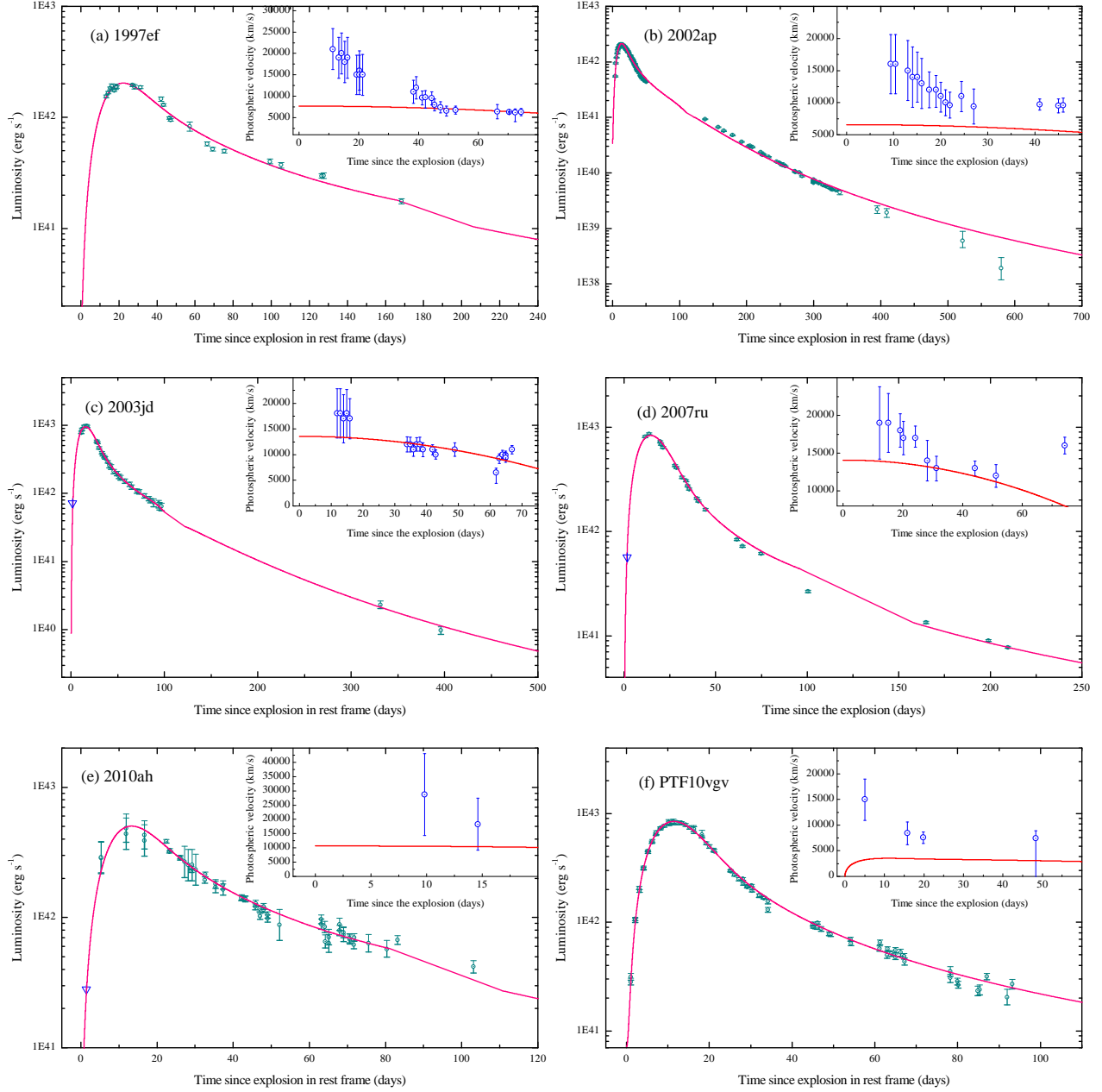


FIG. 9.— Light curves and velocity evolution of the SNe (except for SN 2007bg) in Figures 1 and 2 reproduced by the pure-magnetar model.

Chakraborti, S., Soderberg, A., Chomiuk, L., et al. 2015, *ApJ*, 805, 187  
 Chatzopoulos, E., Wheeler, J. C., & Vinko, J. 2012, *ApJ*, 746, 121  
 Chen, T. W., Smartt, S. J., Jerkstrand, A., et al. 2015, *MNRAS*, 452, 1567  
 Corsi, A., Ofek, E. O., Frail, D. A., et al. 2011, *ApJ*, 741, 76  
 Corsi, A., Ofek, E. O., Gal-Yam, A., et al. 2012, *ApJL*, 747, L5  
 Dai, Z. G., Wang, S. Q., Wang, J. S., Wang, L. J., & Yu, Y. W. 2016, *ApJ*, 817, 132  
 Dong, S. B., Shappee, B. J., Prieto, J. L., et al. 2016, *Sci*, 351, 257  
 Filippenko, A. V. 1997, *ARA&A*, 35, 309

Foley, R. J., Pappenkova, M. S., Swift, B. J., et al. 2003, *PASP*, 115, 1220  
 Galama, T. J., Vreeswijk, P. M., van Paradijs, J., et al. 1998, *Natur*, 395, 670  
 Hu, J. Y., Qiu, Y. L., Qiao, Q. Y., et al. 1997, *IAUC*, 6783, 1  
 Inserra, C., Smartt, S. J., Jerkstrand, A., et al. 2013, *ApJ*, 770, 128  
 Iwamoto, K., Nakamura, T., Nomoto, K., et al. 2000, *ApJ*, 534, 660  
 Janka, H.-T., Melson, T., & Summa, A. 2016, *ARNPS*, 66, 341  
 Kasen, D., & Bildsten, L. 2010, *ApJ*, 717, 245  
 Kashiwayama, K., Murase, K., Bartos, I., et al. 2016, *ApJ*, 818, 94



- Leloudas, G., Fraser, M., Stone, N. C., et al. 2016, *NatAs*, 1, E2
- Liu, L. D., Wang, S. Q., Wang, L. J., et al. 2017, *ApJ*, submitted
- Liu, Z., Zhao, X. L., Huang, F., et al. 2015, *RAA*, 15, 225
- Lunnan, R., Chornock, R., Berger, E., et al. 2016, *ApJ*, 831, 144
- Lyman, J. D., Bersier, D., & James, P. A. 2014, *MNRAS*, 437, 3848
- Maeda, K., Mazzali, P. A., Deng, J. S., et al. 2003, *ApJ*, 593, 931
- Margutti, R., Milisavljevic, D., Soderberg, A., et al. 2014, *ApJ*, 797, 107
- Margutti, R., Soderberg, A. M., Wieringa, M. H., et al. 2013, *ApJ*, 778, 18
- Mazzali, P. A., Deng, J. S., Maeda, K., et al. 2002, *ApJL*, 572, L61
- Mazzali, P. A., Iwamoto, K., & Nomoto, K. 2000, *ApJ*, 545, 407
- Mazzali, P. A., Kawabata, K. S., Maeda, K., et al. 2007, *ApJ*, 670, 592
- Mazzali, P. A., Walker, E. S., Pian, E., et al. 2013, *MNRAS*, 432, 2463
- Metzger, B. D., Margalit, B., Kasen, D., Quataert, E. 2015, *MNRAS*, 454, 3311
- Milisavljevic, D., Margutti, R., Parrent, J. T., et al. 2015, *ApJ*, 799, 51
- Modjaz, M., Blondin, S., Kirshner, R. P., et al. 2014, *AJ*, 147, 99
- Modjaz, M., Liu, Y. Q., Bianco, F. B., & Graur, O. 2016, *ApJ*, 832, 108
- Murase, K., Kashiyama, K., Kiuchi, K., & Bartos, I. 2015, *ApJ*, 805, 82
- Mösta, P., Ott, C. D., Radice, D., et al. 2015, *Natur*, 528, 376
- Nakamura, T., Mazzali, P. A., Nomoto, K., & Iwamoto, K. 2001, *ApJ*, 550, 991
- Nicholl, M., Smartt, S. J., Jerkstrand, A., et al. 2014, *MNRAS*, 444, 2096
- Nishimura, N., Takiwaki, T., & Thielemann, F.-K. 2015, *ApJ*, 810, 109
- Olivares, E., F., Greiner, J., Schady, P., et al. 2015, *A&A*, 577, A44
- Ostriker, J. P., & Gunn, J. E. 1971, *ApJL*, 164, L95
- Patat, F., Cappellaro, E., Danziger, J., et al. 2001, *ApJ*, 555, 900
- Pignata, G., Stritzinger, M., Soderberg, A., et al. 2011, *ApJ*, 728, 14
- Poznanski, D., Ganeshalingam, M., Silverman, J. M., & Filippenko, A. V. 2011, *MNRAS*, 415, L81
- Rakavy, G., & Shaviv, G. 1967, *ApJ*, 148, 803
- Sahu, D. K., Tanaka, M., Anupama, G. C., et al. 2009, *ApJ*, 697, 676
- Sanders, N. E., Soderberg, A. M., Valenti, S., et al. 2012, *ApJ*, 756, 184
- Schlaflly, E. F., & Finkbeiner, D. P. 2011, *ApJ*, 737, 103
- Schlegel, D. J., Finkbeiner, D. P., & Davis, M. 1998, *ApJ*, 500, 525
- Smartt, S. J. 2009, *ARA&A*, 47, 63
- Soderberg, A. M., Chakraborti, S., Pignata, G., et al. 2010, *Natur*, 463, 513
- Suwa, Y., & Tominaga, N. 2015, *MNRAS*, 451, 282
- Thompson, T. A., Chang, P., & Quataert, E. 2004, *ApJ*, 611, 380
- Tomita, H., Deng, J. S., Maeda, K., et al. 2006, *ApJ*, 644, 400
- Umeda, H., & Nomoto, K. 2008, *ApJ*, 673, 1014
- Valenti, S., Benetti, S., Cappellaro, E., et al. 2008, *MNRAS*, 383, 1485
- Walker, E. S., Mazzali, P. A., Pian, E., et al. 2014, *MNRAS*, 442, 2768
- Wang, L. J., Dai, Z. G., Liu, L. D., & Wu, X. F. 2016a, *ApJ*, 823, 15
- Wang, L. J., Han, Y. H., Xu, D., et al. 2016b, *ApJ*, 831, 41
- Wang, L. J., Wang, S. Q., Dai, Z. G., et al. 2016c, *ApJ*, 821, 22
- Wang, L. J., Yu, H., Liu, L. D., et al. 2016d, *ApJ* accepted, (arXiv:1610.09061)
- Wang, S. Q., Liu, L. D., Dai, Z. G., Wang, L. J., & Wu, X. F. 2016e, *ApJ*, 828, 87
- Wang, S. Q., Wang, L. J., Dai, Z. G., & Wu, X. F. 2015a, *ApJ*, 799, 107
- Wang, S. Q., Wang, L. J., Dai, Z. G., & Wu, X. F. 2015b, *ApJ*, 807, 147
- Wheeler, J. C., Yi, I., Höflich, P., & Wang, L. 2000, *ApJ*, 537, 810
- Woosley, S. E. 2010, *ApJL*, 719, L204
- Woosley, S. E., & Bloom, J. S. 2006, *ARA&A*, 44, 507
- Yan, L., Quimby, R., Ofek, E., et al. 2015, *ApJ*, 814, 108
- Young, D. R., Smartt, S. J., Valenti, S., et al. 2010, *A&A*, 512, A70